ELSEVIER

Quaternary Science Reviews 26 (2007) 3118–3133

QSR

Terrigenous input response to glacial/interglacial climatic variations over southern Baja California: a rock magnetic approach

Cécile L. Blanchet*, Nicolas Thouveny, Laurence Vidal, Guillaume Leduc, Kazuyo Tachikawa, Edouard Bard, Luc Beaufort

CEREGE-CNRS-Université Paul Cézanne Aix Marseille III, Europôle Méditerranéen de l'Arbois, BP80, 13545 Aix en Provence Cedex 04, France

Received 5 April 2007; received in revised form 25 June 2007; accepted 14 July 2007

Abstract

The sediments deposited off south-western Baja California have recorded millennial-scale fluctuations in biogenic compounds and trace metals accumulation during the last glacial period [Ortiz, J.D., O'Connell, S.B., DelViscio, J., Dean, W.E., Carriquiry, J.D., Marchitto, T., Zheng, Y., van Geen, A., 2004. Enhanced marine productivity off western North America during warm climate intervals of the past 52 ky. Geology 32, 521–524; Dean, W.E., Zheng, Y., Ortiz, J.D., van Geen, A., 2006. Sediment Cd and Mo accumulation in the oxygen-minimum zone off western Baja California linked to global climate over the past 52 ka. Paleoceanography 21, PA4209]. Since the variations in trace metals concentration appear to result from dilution with nonbiogenic matter, the variability of the terrigenous sedimentation needs to be addressed. Therefore, we performed rock magnetic and geochemical analysis on a 38 m-long sediment core collected from the slope off Baja California. The temporal framework provided by ^{14}C dating and identification of palaeoclimatic transitions allows assigning the sequence to the last glacial–interglacial cycle (~last 120 ka). The comparison of magnetic and geochemical properties led to retain the hypothesis of a primary modulation of iron oxides quantity and quality by terrigenous input variations, with a secondary diagenetic amplification. Two magnetic mineral input regimes are distinguished: (i) magnetic susceptibility variations reveal changes in titano-magnetite concentration related to fluvial transport of the terrigenous fraction; (ii) coercivity changes allow detecting variations of hematite or goethite concentrations, minerals generally issued from aeolian deflation of weathered rock surfaces. These two regimes are paced by two distinct climatic forcing: the millennial-scale changes in titano-magnetite input are related to the northern hemisphere climatic variability whilst the record of wind-blown magnetic mineral input contains its major power in the precessional frequency band, with higher input during low insolation periods (and conversely). This record highlights the great sensibility of this region to high and low latitudes climatic regimes.
© 2007 Elsevier Ltd. All rights reserved.

1. Introduction

Studies of sedimentary dynamics on continental margins have revealed their great potential for detailed reconstructions of palaeoclimatic and palaeoceanographic variations during Plio-Pleistocene times. In particular, the variability of the continental climate can be traced by analysing the characteristics of terrigenous sedimentation in continuous sedimentary sequences from continental margins (Heusser, 1995; Peterson et al., 2000). Moreover, the reconstruction of both climatic and oceanic regimes from one single sedimentary sequence allow investigating their potential linkages and compare their respective responses to large-scale climatic forcing (e.g. Herbert et al., 2001; Jennerjahn et al., 2004).

The magnetic properties of the sediments, measured by nondestructive, rapid and highly sensitive methods, constitute a powerful tool to characterise the terrigenous compounds dynamics. They depend on the nature, concentration and grain size of the terrigenous and/or authigenic ferromagnetic (*sensu lato*) fraction present in the sediment, i.e. ferrimagnetic iron oxides (titano-magnetite), antiferromagnetic iron oxides (haematite, limonite), hydroxides (goethite) or ferrimagnetic authigenic sulphides

*Corresponding author. Present address: Department of Geophysics, Universität Bremen, Fachbereich Geowissenschaften, Postfach 330440, D-28334 Bremen, Germany. Tel.: +49 421 128 3944; fax: +49 421 218 8671.

E-mail address: blanchet@uni-bremen.de (C.L. Blanchet).

0277-3791/$ - see front matter © 2007 Elsevier Ltd. All rights reserved.
doi:10.1016/j.quascirev.2007.07.008

(Maher and Thompson, 1999 and chapter therein). Iron oxi-hydroxides have rather different bulk densities, conditioning different transport paths: the heaviest, Ti-magnetite, is mainly carried by rivers whilst the lightest, haematite (limonite) and goethite, are mainly carried by winds (Thompson and Oldfield, 1986; Maher and Hounslow, 1999).

Here we present magnetic and geochemical properties of a sedimentary sequence collected on the Baja California margin (23°N). Previous studies carried out on neighbouring cores have related the temporal variability of the organic carbon, benthic foraminifera (used as proxies of primary productivity in the surface waters) and trace metals concentrations to the Northern Hemisphere climatic variability of the last glacial period (Ortiz et al., 2004; Dean et al., 2006). In addition, mass accumulation rates of organic carbon, molybdenum and cadmium recently computed by Dean et al. (2006) have shown that the variations of their contents were significantly affected by dilution with nonbiogenic matter. It therefore appears essential to characterise the rhythms of the terrigenous input (potentially discriminated between aeolian and fluvial input), with regards to the variations of the oceanological regimes.

2. Present oceanic and climatic context

The Baja California peninsula lies in the subtropical region, at the boundary between the NE Pacific Ocean and the North American continent. This strip of land separating the Gulf of California from the Pacific Ocean is ~100 km wide. It is characterised by a general upward slope from the west to the east, with a mountain range (from 800 to 2000 m altitude) overhanging the Gulf of California. This general topography is cut by an extensive and intensive fluvial network, transporting detritus originating from erosion of arid and denudated surfaces to the continental shelf (Fig. 1a). The climate of Baja California strongly contrasts in time and space, with a winter precipitation regime in the North and a summer precipitation regime in the South (Fig. 1b). Prevailing winds blow from the north-west along the Pacific Coast (Zaitsev et al., 2003) (Fig. 1c). In summer, the climate of the southern Baja California is characterised by limited precipitation (~15 cm/year) and weak winds due to the development over the continent of a cyclonic cell related to the North Mexican Monsoon (Fig. 1b,c). These climatic conditions result from the northward migration of the intertropical convergence zone (ITCZ). In winter, the region is arid and strong NW winds are generated between the high pressure cell over the ocean and the low pressure cell over the continent (Fig. 1c), inducing an intense upwelling that activates the biological surface production (Thomas et al., 2001).

The studied region lies at the southern intersection of three surface currents with strong seasonal variability: the California current (CC) is a cold southward surface current, while the Davidson Surface Counter-Current and the California Under-Current are warm northward currents (Lynn and Simpson, 1987) (Fig. 1c). At intermediate depth, the North Pacific Intermediate Waters (NPIW) are characterised by low temperature, low salinity (Talley, 1993) and low O_2 contents. More precisely, between 300 and 800 m, low concentrations of dissolved oxygen ($[O_2] < 5\,\mu mol/l$, van Geen et al., 2003) are related to the Eastern Pacific oxygen minimum zone (OMZ), relatively constant in strength and bathymetric extension.

3. Core description

Core MD02-2508 was retrieved on the continental slope off south Baja California peninsula (23°27.91′ N, 111°35.74′ W, water depth 606 m; Fig. 1) by the R.V. *Marion-Dufresne* during the coring campaign MD126-MONA (IMAGES VIII, summer 2002). The 38 m-long sediment column was collected with the Calypso giant piston corer. At present, the coring site lies at the depth of the Eastern Pacific OMZ. The cored sediments are formed of hemipelagic silty-clayey muds composed of mixed biogenic and minerogenic fractions. Several depth intervals are characterised by alternating light-coloured biogenic compounds (diatoms and foraminifera tests) and dark-coloured organic and terrigenous compounds, defining laminae couplets at millimetric to centimetric scales. The non-laminated intervals consist of homogenous green-grey silty clays exhibiting bioturbation patterns.

On board measurements of physical properties of the sediments show that lithological changes are associated to changes in colour and density (i.e. porosity): the dark-coloured laminated facies has weak density, whilst light-coloured non-laminated facies has stronger density (Beaufort et al., 2002). In a nearby coring site, sediment reflectance factors defined by multivariate analysis were correlated with the organic carbon and carbonate contents (Ortiz et al., 2004).

4. Analytical methods

After a 3-months storage at 4 °C, core MD02-2508 was subsampled using U-channels (1.5 m long, 4 cm^2 section). Discrete specimens were also collected at several depth intervals for complementary rock magnetic and geochemical analyses. Magnetic parameters were measured at the palaeomagnetic laboratory of the CEREGE (Aix-en-Provence, France). Organic, carbonate and absolute elemental contents were also measured there.

4.1. Magnetic parameters

The low field volume magnetic susceptibility (K) was measured every 2 cm on the U-channels using a Bartington MS2 susceptibility meter and a pass-through MS2B probe. K is expressed in 10^{-5} SI.

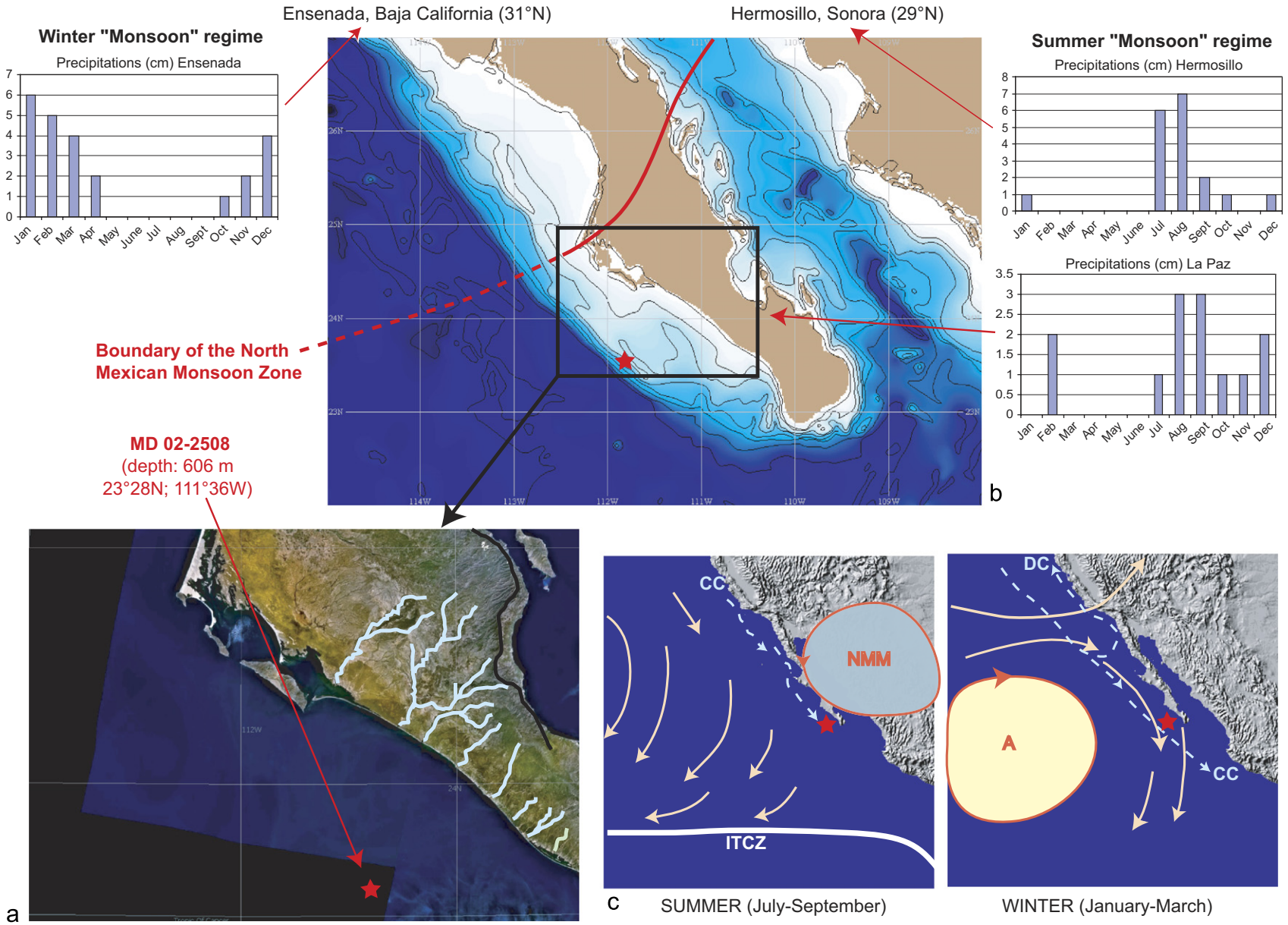

Fig. 1. Location of core MD02-2508 (23.28°N, 111.36°W, red star) and climate of the Southern Baja California margin (Mexico). (a) Physiography of the Baja California peninsula: blue lines represent the rivers, black line sets the limit of the drainage basin, (b) bathymetric map of Baja California margin, with precipitation data for the two climatic regimes: winter "monsoon" regime in the North (Ensenada) and summer "monsoon" regime in the South (Hermosillo and La Paz). Precipitation data (averaged over 30 years) from Weatherbase (http://www.weatherbase.com/). (c) Principal atmospheric features (wind directions: solid arrows) and surface oceanic currents (dashed arrows) for boreal summer and boreal winter. NMM: North Mexican (summer) Monsoon, ITCZ: Intertropical Convergence Zone, A: high pressure cell, CC: Californian Current and DC: Davidson Current.

In order to distinguish different mineralogic and granulometric fractions, two types of remanent magnetisations were artificially imparted: (1) an anhysteretic remanent magnetisation (ARM) was created in alternating field of 100 mT (peak amplitude) superimposed to a 0.1 mT steady field; (2) isothermal remanent magnetisations (IRM) were created by passing the samples into permanent annular magnets (Halbach cylinders, Rochette et al., 2001) producing fields of 0.3 and 1 T. The IRM_{1T} is here considered as a reasonable approximation of the saturation IRM (SIRM). The backfield IRM was imparted at −0.3 T in order to saturate the magnetite. ARM and IRM were measured at 2 cm intervals using a superconducting (SQUID) pass-through magnetometer (2G 760R) whose sensor geometry imposes a smoothing of the magnetisation signal equivalent to a ~5 cm sliding averaging window. Stepwise alternating field (AF) demagnetisation was performed at peak values of 20, 30 and 40 mT. Volume magnetisations are expressed in $A \cdot m^{-1}$.

Hysteresis loops and demagnetisation of the saturation isothermal remanent magnetisation (peak field of 1 T) were performed on selected samples with a gradient force Micromagnetometer (Princeton Measurements Corporation, model Micromag 3900).

4.2. Relative elemental content: XRF measurements

The relative content of certain major and trace elements were measured every 2 cm using a X-ray Fluorescence scanner (Avaatech™, RCOM Bremen). The analyses were performed on the bulk sediment samples of selected U-channels and integrate a 1-cm^2 area. Under the influence of incident X-rays, each atom species produces a specific energy and wavelength spectrum. The concentration determines the intensity of the wavelength peak (Jansen et al., 1998). The settings were adjusted at 10 kV in order to detect the elements ranging from aluminium (Al) to iron (Fe), including titanium (Ti), calcium (Ca), silicon (Si), sulphur (S) and potassium (K). Each individual power spectrum is transformed by a computer-assisted deconvolution process into relative contents expressed in counts per second. Two depth intervals were analysed: 276–726 cm (Sections 3–5) marked by a clear transition between laminated and bioturbated sediments which corresponds to the last glacial–interglacial transition and 1176–1326 cm (Section 9) characterised by alternations of laminated and non-laminated intervals occurring during Marine Isotope Stage (MIS) 3.

4.3. Absolute elemental contents: ICP-OES measurements

The absolute concentrations of Fe, Ti and Ca were analysed in 16 bulk sediments samples by Inductively Coupled Plasma Optical Emission Spectrometer (ICP-OES, Jobin Yvon Ultima C). Prior to ICP-OES measurements, the samples were totally dissolved using HF (23 M), HNO_3 (15 M) and HCl (12 M). Blank levels of the total digestion were below detection limit. Estimated analytical uncertainty based on the measurement of geostandard MAG-1 is better than 5%.

4.4. Percentages of organic carbon and carbonate

Total carbon and total organic carbon contents (TC and TOC, respectively) were measured on a CNS elemental analyser (FISONS 1500) every 10 cm, from 0 to 1800 cm following the procedure of Verardo et al. (1990). The organic carbon concentrations were measured after dissolution of the calcium carbonates by adding a 1 M solution of HCl to the dry sediment. Each TOC value is an average of two measurements. The standard used for TC and TOC is an Acetanilide powder (C_8H_9NO, containing 71.09% carbon). The accuracy and precision of measurements are routinely checked by successive analysis of an internal marine sediment standard that contains 2.2% of carbon. The $CaCO_3$ percentage has been calculated using the following equation:

$$\%CaCO_3 = (\%TC - \%TOC) * 8.33.$$

5. Guidelines for interpretation of magnetic parameters

The magnetic susceptibility and the artificially imparted magnetisations (ARM, IRM, etc.) depend on the concentration, mineralogical nature and grain size of the magnetic fraction. Their raw values and ratios have been widely used as tracers of mineral sources and depositional/diagenetic environments (e.g. Maher and Thompson, 1999). A short review of their interpretation and their limitations is provided here and summarised in Table 1.

5.1. Tracers of concentration and nature of terrigenous magnetic grains

The bulk magnetic susceptibility (K) is influenced by all sedimentary fractions. However, the contributions of diamagnetic minerals (e.g. calcite and silica) and paramagnetic minerals (iron bearing silicates and clay minerals) are negligible in comparison with that of the ferromagnetic minerals *sensu lato* (i.e. iron oxides, iron hydroxides and iron sulphides). Among those, magnetite (Fe_3O_4) and titano-magnetite ($Fe_{3-x}Ti_xO_4$) have K values 10–100 times stronger than others. For a given magnetic mineral, K also varies with grain size: stronger for large grains, weaker for small grains. Therefore, in sediments K is primarily dependent on the concentration of the coarse Ti-magnetite. Remanent magnetisations such as ARM and IRM are only carried by ferromagnetic minerals: ARM and backfield $IRM_{-0.3T}$ only concern low coercivity phases (e.g. Ti-magnetite), whereas the IRM acquired above 0.3 T concerns imperfect anti-ferromagnetic minerals, e.g. haematite (αFe_2O_3) and goethite (FeOOH). Concentration variations of these minerals can be traced by the hard IRM

Table 1
Interpretation guidelines for the magnetic parameters (see text for further information and references)

Parameter	Interpretation	Possible bias
Concentration indicators		
Magnetic susceptibility *K*lf (absolute)	All minerals mainly coarse Ti-magnetite	Increase with greigite and/or pyrrhotite Biased by coarse Ti-magnetite
ARM (absolute)	Low coercivity ferrimagnets mainly Ti-magnetite	
SIRM (absolute)	Ferrimagnets, mainly Ti-magnetite	
IRM-0,3T (absolute)	Ti-magnetite	
Mineralogy indicators		
HIRM (absolute)	High coercivity minerals (anti-ferromagnets: haematite + goethite)	Greigite or pyrrhotite
SIRM/*K* (high values) (relative)	Ferrimagnetic sulphides (greigite + pyrrhotite)	
Magnetic grain size indicators (theoretical response)		
ARM_{30mT}/ARM		
IRM_{30mT}/IRM		Increase with greigite or pyrrhotite
ARM/*K*	Increase when grain size decreases	
SIRM/*K*		
ARM/SIRM		Decrease with greigite or pyrrhotite

(HIRM) calculated as follows:

$$HIRM = (SIRM + IRM_{-0.3\ T})/2.$$

Complementary information is drawn from hysteresis cycles: saturation fields H_{sat} vary from 0.2 T for Ti-magnetite, up to several Tesla for haematite; coercive fields H_c and H_{cr} constitute key parameters to discriminate ferromagnetic and antiferromagnetic minerals.

5.2. Proxies of magnetic particle size and their limitations

If Ti-magnetite is the dominant ferrimagnetic mineral, the normalised parameters ARM/IRM, IRM/*K*, ARM/*K* and $ARM_{AF20\ mT}/ARM$ are grain size dependent: they increase when the grain size decreases. Few of them must be considered with caution: (i) for the magnetite size ranges [0.01–2 μm] and [10–100 μm], the ARM/SIRM ratio follows contradictory trends (King et al., 1983); (ii) authigenic ferrimagnetic sulphides (greigite, pyrrhotite) strongly influence the $ARM_{20\,mT}/ARM$ and SIRM/*K* ratios (Roberts, 1995; Peters and Thompson, 1998) (Table 1).

6. Results

6.1. Sedimentary magnetism results

As indicated above, the magnetic signals (and their environmental interpretations) can be biased by the presence of authigenic ferrimagnetic sulphides. It is therefore necessary to evaluate their possible contribution to the magnetic fraction in core MD02-2508. Most *K* values are between -2.10^{-5} and 5.10^{-5} SI, except at the base of the core (3798–3866 cm) where they reach 10.10^{-5} SI (Fig. 2). The SIRM and SIRM/*K* profiles are affected by spikes at ~100 cm, ~1082 cm, ~3449 cm, ~3640 cm and 3800–3850 cm indicating that ferrimagnetic sulphides are present in the laminated facies (Fig. 2). These layers carrying high SIRM/K ratios were disregarded and eliminated from the following figures in order to fully express the small and medium amplitude variability of the magnetic signal.

Three remarks arise from Fig. 3: (i) magnetic mineral concentration is weak (maximum *K* values reach 5×10^{-5} SI units, $ARM_{20\,mT}$ and HIRM fall between 10^{-7} and 10^{-5} A/m, SIRM and $IRM_{-0.3\ T}$ fall between 10^{-5} and 10^{-4} A/m); (ii) low and high values of *K*, ARM, IRM and HIRM are recorded in the laminated and non-laminated facies, respectively; (iii) the magnetic grain size indicator $ARM_{20\,mT}/ARM$ ratio is in anti-phase with the ARM/*K* and ARM/SIRM ratios, particularly in the laminated facies, which leads to contradictory interpretations and points out the need to test their respective validity as magnetic mineral grain size index.

From the rock-magnetic point of view, the sedimentary sequence can be divided in three parts (Fig. 3):

- Part I (0–500 cm) is continuously laminated, with weak magnetic concentrations, as indicated by rather low values of ARM, IRM and HIRM. However, ARM and IRM peaks at 100 and 400 cm depth point out ferrimagnetic enrichment. High ARM/*K* and ARM/SIRM ratios are in contradiction with low $ARM_{20\,mT}/ARM$ ratio.
- The transition between parts I and II (transition I/II) is marked at 500 cm by the abrupt interruption of the laminated series and by an increase of the magnetic minerals concentration. The abrupt increase of *K* (500–600 cm) is accompanied by a gradual increase of ARM, IRM and HIRM, starting at 700 cm. Magnetic ratios also indicate large amplitude variations during this transition, with a distinct feature at 700 cm consisting in low $ARM_{20\,mT}/ARM$ values and strong ARM/*K* and ARM/SIRM values.
- In part II (700–2000 cm) laminated and non-laminated facies alternate. Relatively high *K*, ARM and IRM values indicate a strong magnetic concentration. The laminated series are characterised by abrupt decreases of the magnetic concentration revealing rapid return to sedimentary conditions described for part I. A particular feature of part II consists in oscillations of ~600 cm wavelength in ARM, IRM and HIRM signals. Again, variations of the $ARM_{20\,mT}/ARM$ ratio contradict the variations of the ARM/*K* and ARM/SIRM ratios.
- The transition between parts II and III (2000–2400 cm) documents a gradual change from high to low magnetic

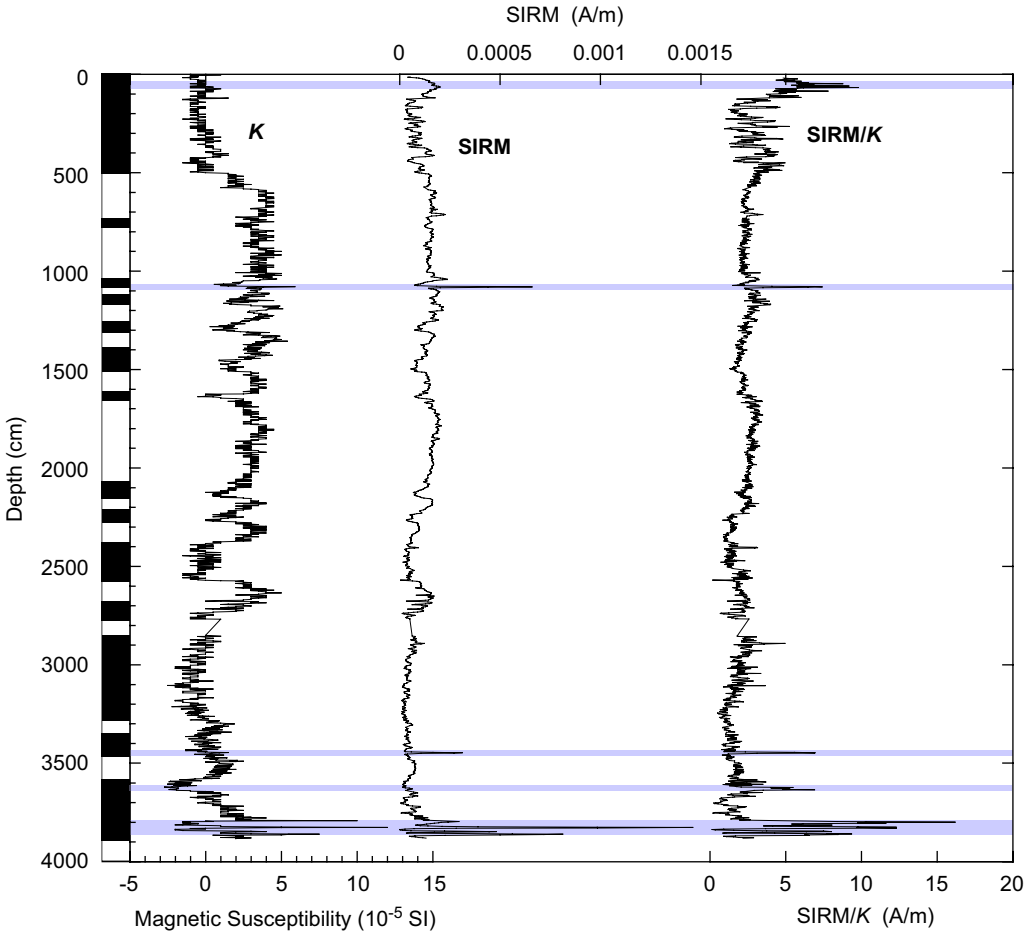

Fig. 2. Ferrimagnetic sulphides detection. Comparison between magnetic susceptibility (K), saturation IRM (SIRM) and the ratio SIRM/K on the depth scale (cm). Values of SIRM/K higher than 5 A/m are underlined. In these levels, enrichments of ferrimagnetic sulphides (greigite, pyrrhotite) are suspected. Laminated intervals are represented as black rectangles (left panel).

concentrations, marked by two abrupt decreases at 2120 and 2260 cm in laminated facies alternating with sharp increases at 2170 and 2300 cm in non-laminated facies.

- Part III is almost entirely laminated and characterised by low magnetic concentrations except in one non-laminated interval between 2600 and 2750 cm. K presents larger amplitude variations noticeably between 3200 and 3900 cm. The phase opposition between $ARM_{20\,mT}$/ARM and ARM/K ARM/SIRM signals is particularly well expressed.

The contradictory behaviour of magnetic grain size indices has been further investigated using the grain size distribution of 14 samples selected in contrasted sedimentary facies, measured using a laser granulometer (Malvern Mastersizer). Since remanent magnetisation is carried by the clayey (<4 μm) and silty (4–63 μm) fractions, the most relevant grain size index is the clay/silt ratio (rather than classical parameters like mode and median, which concern the whole grain size range). Maximum values of this ratio are evidenced in the non-laminated transition I/II, whilst minimum values are documented in laminated parts I and III (Fig. 4). The $ARM_{20\,mT}$/ARM ratio can be considered as the most reliable proxy of the grain size of the magnetic fraction because it follows the same trend and is reasonably correlated to the clay/silt ratio ($R = 0.57$) (Fig. 4). On the contrary, the two other magnetic grain size indicators showed negative correlations with the bulk grain size parameters. $ARM_{20\,mT}$/ARM profile then provides a continuous and high-resolution analogue of the granulometric variations of the terrigenous fraction along the entire sequence.

Hysteresis cycles document the balance between low and high coercivity minerals in contrasted facies. Low coercivity and low saturation field confirm that Ti-magnetite is dominant in parts I and III (Fig. 5a,b,g,h). Higher coercivity and saturation field suggest significant contributions of haematite and/or goethite in part II (Fig. 5c,d,e,f).

The magnetic records evidence three types of variability: (i) a long term variability of magnetic concentration, mineralogy and grain size (defined by major subdivisions and linked with the lamination patterns); (ii) medium wavelength (~600 cm) oscillations affecting the Ti-magnetite and haematite or goethite concentrations (without direct relation with the occurrence of laminations) and (iii) a short wavelength variability of the concentration of

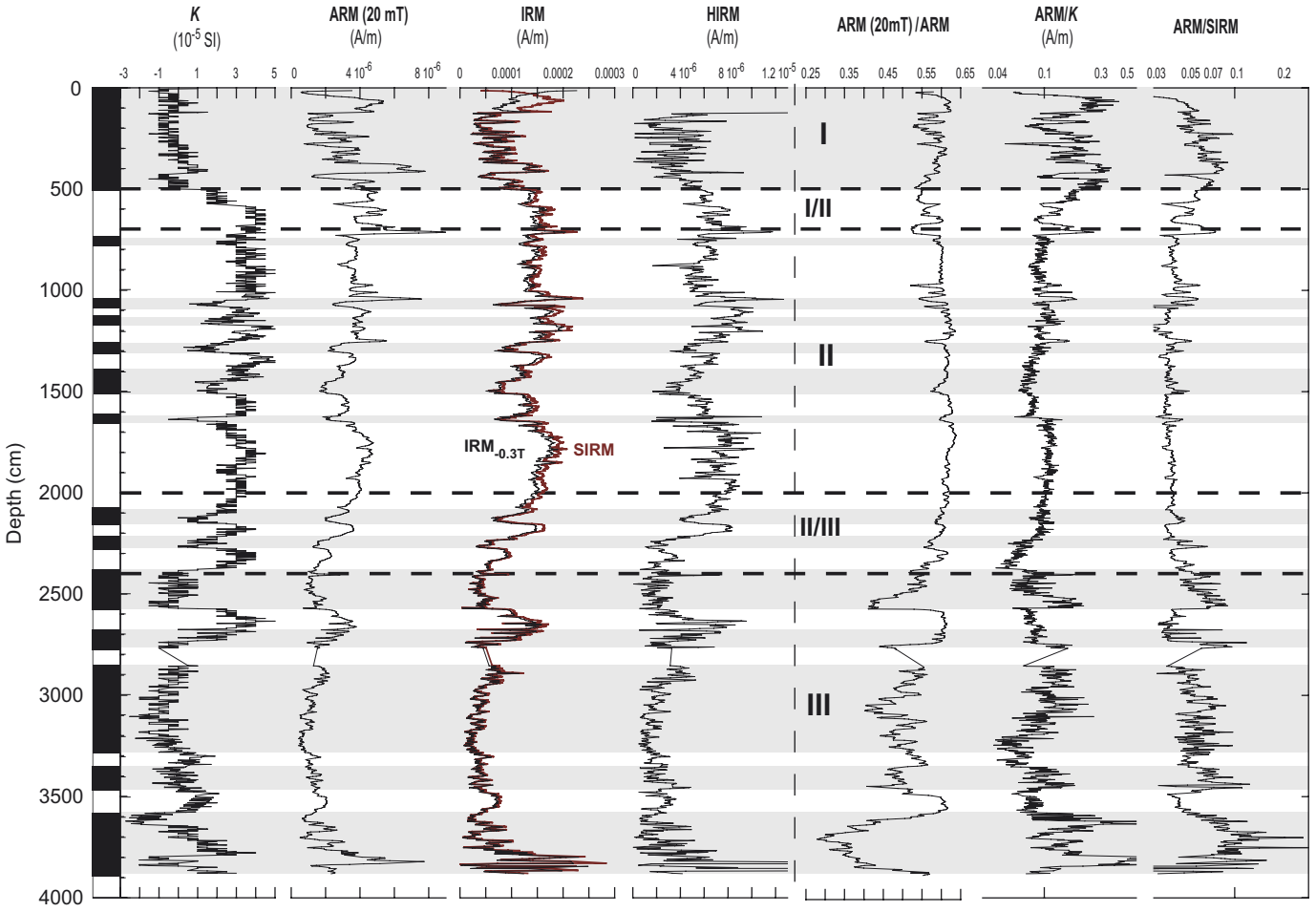

Fig. 3. Magnetic record of core MD02-2508 on the depth scale (cm). Magnetic concentration indices: magnetic susceptibility (K), $ARM_{20\,mT}$, SIRM and $IRM_{-0.3\,T}$, and hard IRM (HIRM); magnetic grain size indices: $ARM_{20\,mT}/ARM$, ARM/K and $SIRM/K$. Laminated intervals are represented as black rectangles (left panel) and underlined as grey bands through the different plots. The magnetic record is divided in three parts (I, II, III) and two transition (I/II, II/III).

both the Ti-magnetite and the haematite and/or goethite (mainly identified in part II and linked with minor laminated units).

6.2. Geochemical results

6.2.1. Organic carbon and carbonates percentages

The total organic carbon (TOC) and calcium carbonate ($CaCO_3$) contents are plotted besides K and HIRM from 0 to 1800 cm (i.e. part I and II, Fig. 6). The TOC content varies from 4 to 15% and $CaCO_3$ percentage from 8 to 40%. The Carbon/Nitrogen ratio suggests that the organic carbon mainly originates from marine algae (data not shown).

Part I records the maximum TOC content ($> 10\%$) and minimum $CaCO_3$ content ($< 30\%$) with several large amplitude and abrupt variations not observed in the magnetic parameter variations. Transition I/II records a TOC decrease and a $CaCO_3$ increase, in parallel with a susceptibility increase. In part II, the TOC and $CaCO_3$ contents are in antiphase and present large and abrupt variations. TOC maxima and $CaCO_3$ minima are recorded in the laminated intervals, also corresponding to lower magnetic concentrations.

6.2.2. Major and trace elements concentrations

Major and trace elements have been measured from two depth intervals: 250–750 cm (part I and transition I/II) and 1100–1300 cm (part II) (Fig. 6). Titanium (Ti), potassium (K) and silicon (Si) are mostly contained in silicates and oxides inherited from erosion of continental rocks. Si and K profiles show a similar trend, inverse to the TOC content (Fig. 6), suggesting that Si is mainly carried by the silicate fraction, although a contribution from biogenic origin cannot be discarded. The abundance of these elements, measured using the XRF methods are similar: Ti ranges from 400 to 1800 counts/s, K and Si range from 500 to 3500 counts/s. Absolute Ti content measured using an ICP-OES on selected bulk samples ranges from 0.15% to 0.28%. Iron (Fe) is about ten times more concentrated: relative values range from 4000 to 16,000 counts/s and absolute concentration range from 1.8% to 2.5% (Fig. 6).

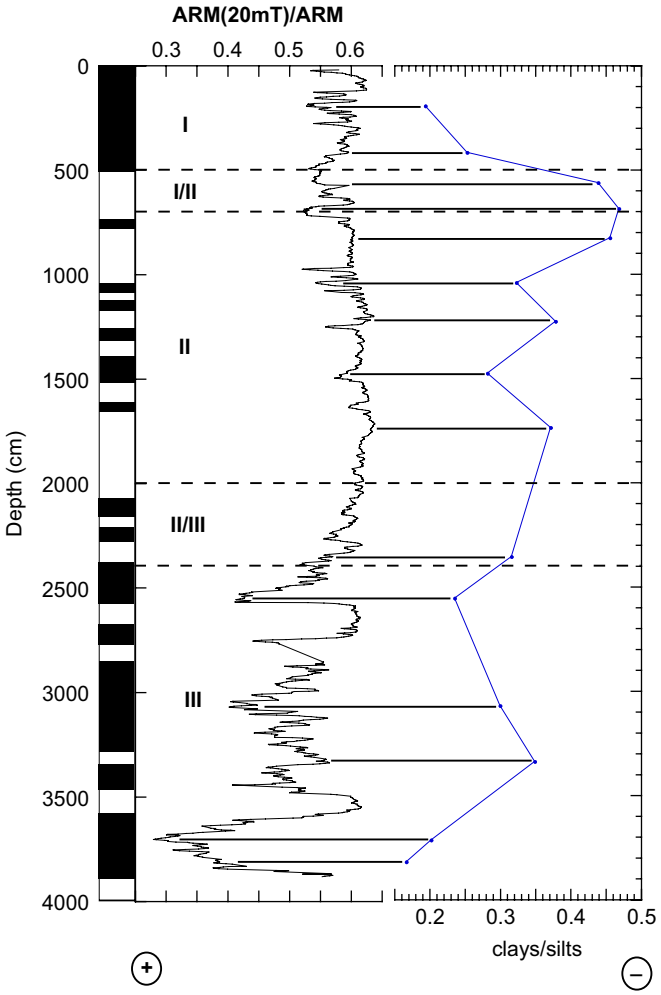

Fig. 4. Comparison of the magnetic grain size indicator $ARM_{20\,mT}/ARM$ with the clay/silts ratio [clays (<4 μm), silts (4–63 μm)] on the depth scale. Principal lithological features are indicated in the left panel, boundaries between parts I, II and III are shown as dotted lines and grain size changes are indicated by ± beneath the plots.

Fe primarily originates from lithogenic sources, such as Fe–Mg silicates, iron oxides and clay minerals. It is associated secondarily with sulphur (S) and phosphorus (P) in authigenic sulphides and phosphates. The relative S content ranges from 500 to 2500 counts/s. The S cycle is mainly influenced by biological activity (organic sulphur and sulphates), that produces, under anoxic conditions, iron sulphides (linked with diagenetic dissolution of iron oxides) or linkages of S and organic compounds (Suits and Arthur, 2000).

In part I, the relative contents of Ti, K, Si and Fe are low, except between 250 and 330 cm. The S content decreases from more than 1500 to less than 1000 counts/s from 300 to 500 cm with a slight increase between 420 and 500 cm (Fig. 6). Transition I/II is marked by an increase of Ti (beginning at ~420 cm), K, Si and Fe (beginning at ~350 cm). These elements reach a plateau of high values between ~600 and 750 cm. Ti values are highly variable, whilst S values are the lowest of the whole sequence. In part II, the concentration of these elements is higher than in part I, reaching peak values in the intervals 1200–1210 cm and 1280–1300 cm. Apart from these peaks, the elemental contents do not co-vary: Ti, Si and Fe are low, K decreases between 1200 and 1280 cm and S increases between 1220 and 1300 cm.

7. Age model

The age model of core MD02-2508 was constructed using 16 Accelerator Mass Spectrometer (AMS) ^{14}C dating (Table 2): 14 were obtained from benthic foraminifera (*Uvigerina peregrina*) and two from planktonic foraminifera (*Globigerinoides ruber*). Following van Geen et al. (1996, 2003), ages obtained on benthic foraminifera were first converted into "equivalent planktonic ages" by taking into account the radiocarbon age of inorganic carbon at core depth. A water mass age of 1500 years was considered, as estimated at 700 m water depth at GEOSECS station 201 (34°N) (Ostlund et al., 1987). For the surface waters, we used the age of 601 ± 53 years, obtained in Baya de Magdalena (23°N, 111°W) by Berger et al. (1966) and confirmed by Ostlund et al. (1987). Since the global ocean surface reservoir age is estimated at 400 years, the 200 years difference (ΔR) is probably due to upwelling of older waters in this region. All ages were corrected from this surface reservoir age and ΔR (Table 2). Ages younger than 25 ka were adjusted on the calibration curve established by Hughen et al. (2004) using the software Calib 5.0 (Stuiver et al., 2005). Older ages were corrected using the equation from Bard et al. (2004). The calibrated ages obtained from both benthic and planktonic foraminifera from the same depth levels differ by ~400–800 years (i.e. samples 435–438 cm and 670–673 cm, Table 2); an arithmetic mean was computed when the 2σ errors overlapped. Ages with overlapping error bars obtained from nearby samples (i.e. at 450–452 cm and at 1101–1126 cm) were also averaged.

Depth to age transformation was performed by linear interpolation between control points (Fig. 7). The calibrated ^{14}C ages are distributed between 470 and 38,300 years and estimated sedimentation rate falls between ~19 and 35 cm/ka. However, a sedimentation rate of ~60 cm/ka obtained in the first 3 m is probably due to a coring-induced elongation (Thouveny et al., 2000). Also, a noticeable increase of sedimentation rate between 550 and 670 cm is documented, corresponding to the 14–18 ka interval. Although the resolution of the ^{14}C dating is not sufficient, no obvious relation between sedimentation rate and lithological changes (laminated/non-laminated) is evidenced (Fig. 7). Apart from these specific intervals, the averaged sedimentation rate of core MD02-2508 (~32 cm/ka) is similar to estimates obtained on neighbouring cores (van Geen et al., 2003; Ortiz et al., 2004), but is less constant (by comparison with the almost constant sedimentation rate recently computed by Marchitto et al., 2007).

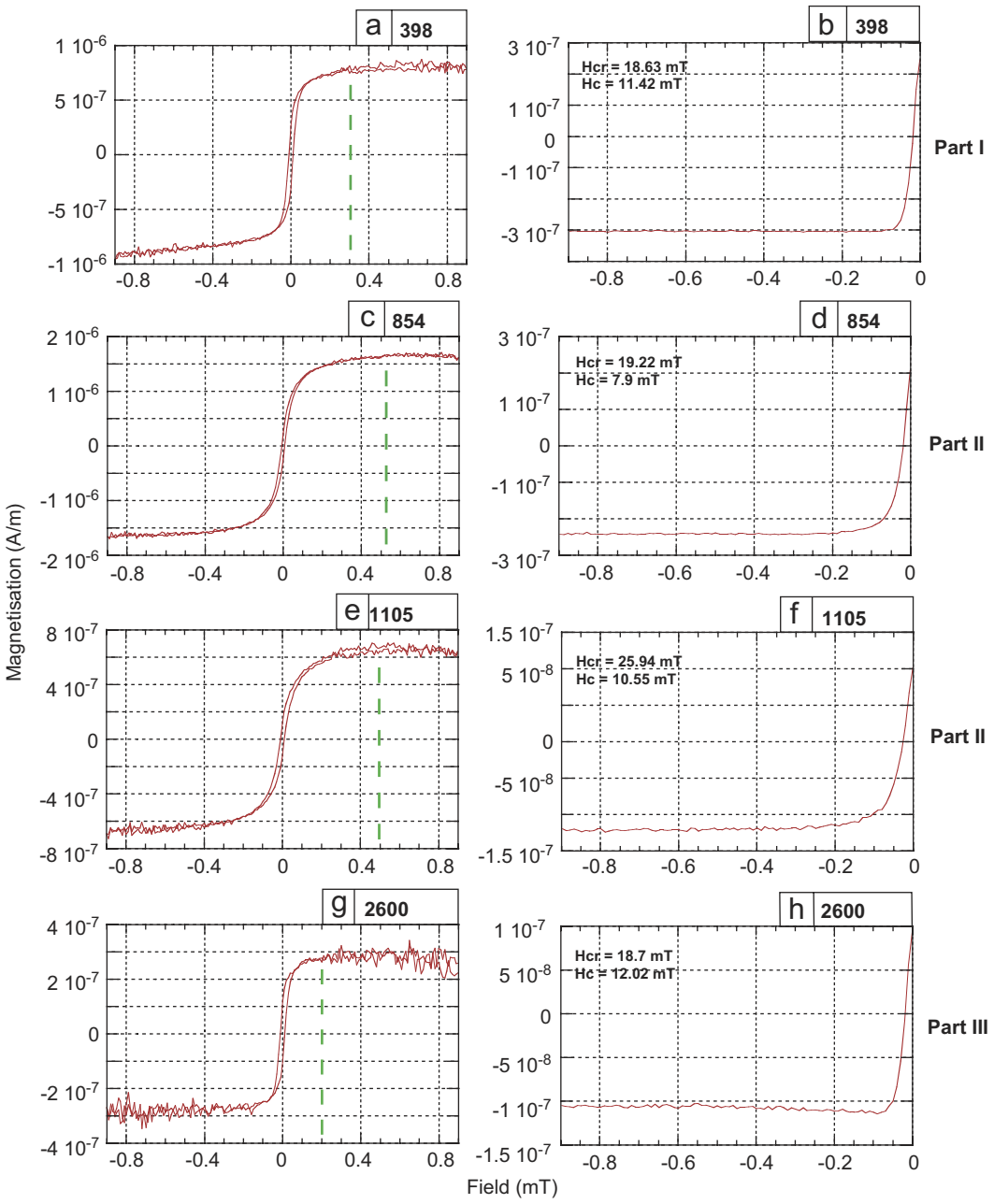

Fig. 5. Hysteresis plots (a,c,e,g) and demagnetisation of saturation remanence curves (b,d,f,h) of four samples representatives for parts I–III. Saturation fields (dotted lines) and coercive fields values (H_c and H_{cr}) are provided. Low MS samples (laminated intervals) (Part I: 398 cm, a,b; Part III: 2600 cm, g,h): saturation fields of 0.2–0.3 T and low coercive fields indicate dominance of Ti-magnetite. High MS samples (non-laminated intervals) (Part II: 854 cm, c,d and 1105 cm, e,f): saturation fields of 0.4–0.5 T and high coercive fields indicate significant contribution of high coercivity minerals, such as haematite, goethite or ferrimagnetic sulphides.

Palaeomagnetic measurements performed all along the core (unpublished data) fulfil the chronological dataset. Large amplitude deviations of the inclination and declination (~60° and ~180°, respectively), between 3830 and 3860 cm provide evidence of the occurrence of a palaeomagnetic excursion (data not shown). The down-core extrapolation based on mean sedimentation rate (computed through the ^{14}C dated section) provides an age of ~114 ka BP for this level, at the transition MIS 5e/5d. The only global magnetic excursion recorded during this time interval is the Blake Event, dated at ~117 ka BP by thermoluminescence in the Chinese loess (Fang et al., 1997). In addition, the fully reversed inclinations, complete rotation of the horizontal component of the vector and two-fold pattern recorded in MD02-2508 are compatible with the signatures already described for the Blake Event (Tric et al., 1991; Thouveny et al., 2004).

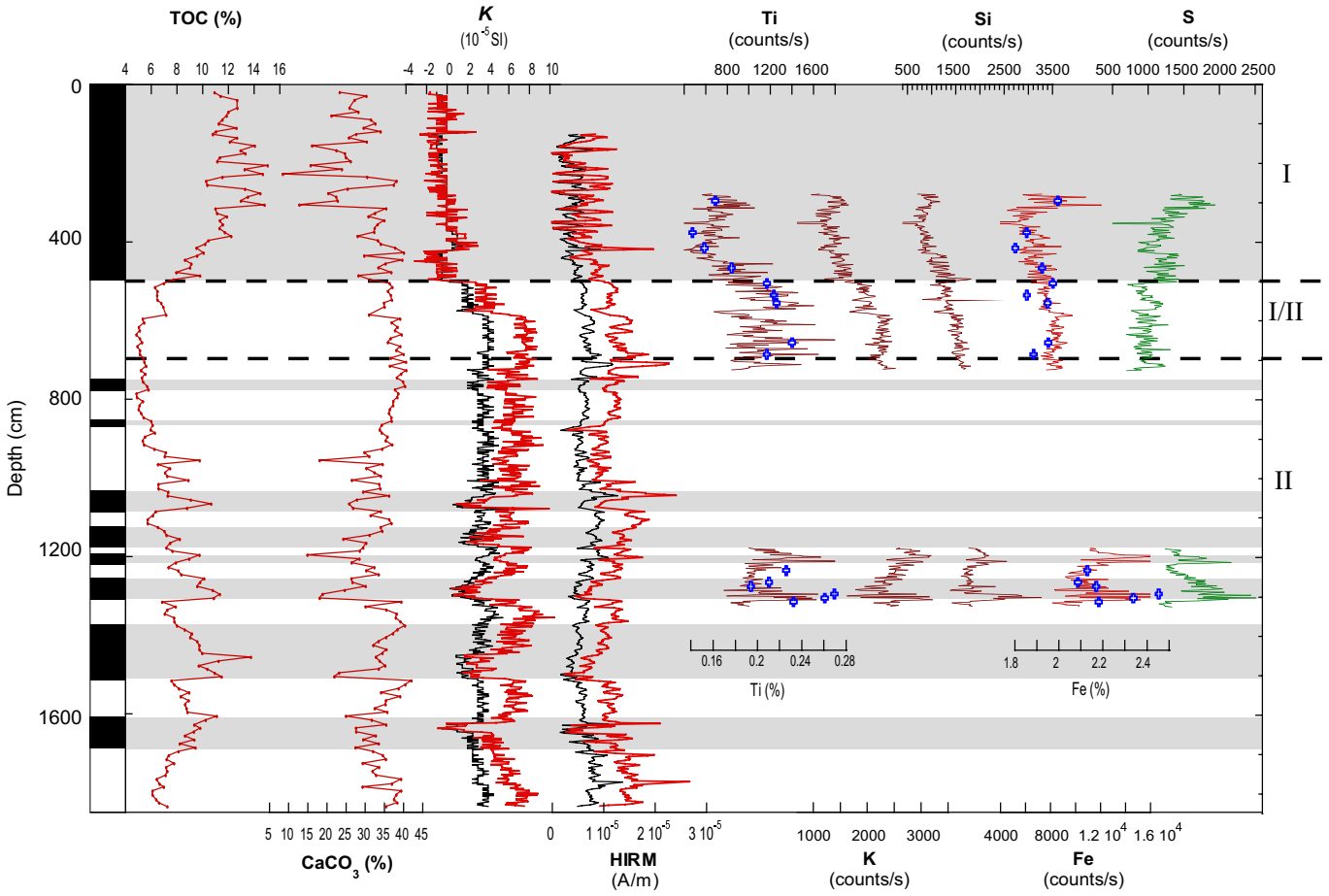

Fig. 6. Magnetic and geochemical records along the upper 1800 cm. Biogenic components: total organic carbon (TOC) and calcium carbonate ($CaCO_3$) percentages. Magnetic concentration indices: magnetic susceptibility (K) and Hard IRM (HIRM), raw (thin black line) and corrected for the dilution effect by $CaCO_3$ and TOC content (thick red line). Relative elemental contents (lines): Titanium (Ti), potassium (K), silicon (Si), iron (Fe) and sulphur (S). Absolute Ti and Fe contents (blue crosses). Boundaries of parts I, II and transition I/II are shown as dotted lines.

8. Discussion

8.1. Modulation of the magnetic signal: terrigenous input, dilution or diagenetic transformation?

One of the main features drawn from Section 6 is the opposition of physical and chemical parameters of laminated and non-laminated sediments. The former presents weak magnetic concentrations, a coarser grain size, weaker signals of terrigenous elements (Ti, K, Si and Fe) and carbonate contents, higher TOC and higher sulphur contents compared to the latter. Therefore, we may propose several interpretations of magnetic minerals concentration changes: (i) dilution of the lithogenic fraction by the biogenic compounds, (ii) dissolution of the magnetic minerals in reducing conditions and (iii) variations of the magnetic mineral input. The respective influences of these processes under varying physico-chemical environments are complementary, as discussed hereafter.

8.1.1. Dilution of magnetic minerals by biogenic fraction

We have corrected the possible effects of dilution on K and HIRM signals by biogenic compounds (such as organic carbon and carbonate) using the formula of Bloemendal et al. (1988):

$$K_{corr} = 100 * K/[100 - (\%CaCO_3 + \%TOC)].$$

The biogenic silica content is considered as negligible in comparison with carbonates and organic carbon (see Section 6.2.2). Comparison of raw and corrected magnetic profiles (Fig. 6) shows that the variability between laminated and non-laminated facies is not only preserved, but is in most cases enhanced. This shows that variations of magnetic parameters are not caused by dilution of terrigenous minerals with biogenic compounds.

8.1.2. Dissolution of Fe–Ti oxi-hydroxides

Dissolution of iron oxides and authigenesis of iron sulphides are activated by high organic matter and low dissolved oxygen concentrations. Dissolved H_2S (produced

Table 2
AMS ^{14}C measurements obtained on biogenic carbonates (foraminifera species, sample depth interval, ^{14}C ages and analytical errors)

Species	Depth (cm)	^{14}C age (yr BP)	Equivalent planktonic ^{14}C age (900 yrs) (yr BP)	^{14}C Age corr. from reserv. age (600 yr) (yr BP)	95.4% (2σ cal age ranges (cal. BP)	Calendar age (cal. BP)
U. peregrina	20	1970±120	1070±120	470±120	250-696	**473±173**
U. peregrina	100	3250±80	2350±80	1750±80	1511-1968	**1740±229**
U. peregrina	317	6080±60	5180±60	4580±60	5026-5569	**5298±272**
U. peregrina	331	6400±90	5500±90	4900±90	5455-5897	**5676±221**
U. peregrina	437	9230±70	8330±70	7730±70	8404-8904	**8896±274**
G. ruber	435-*38*	*8710±100*		*8110±100*	8841-*9435*	
U. peregrina	450	9940±120	9040±120	8440±120	9188-9903	**9433±286**
U. peregrina	452	9800±80	8900±80	8300±80	9107-9534	
U. peregrina	556	13860±90	12960±90	12360±90	14011-14870	**14441±430**
U. peregrina	671	16540±160	15640±160	15040±160	17833-18753	**17910±473**
G. ruber	670-*73*	*15190±100*		*14590±100*	17041-*18013*	
U. peregrina	716	17830±130	16930±130	16330±130	19741-19785	**19785±444**
U. peregrina	811	22180±120	21280±120	20680±120	24401-25378	**24890±489**
U. peregrina	971	30140±270	29240±270	28640±270	33192	**33192**
U. peregrina	1101	35260±290	34360±290	33760±290	38721	**38330**
U. peregrina	1126	34230±450	33330±450	32730±450	37939	

The benthic radiocarbon ages were first converted into "equivalent planktonic ages" by taking into account the ages of the inorganic carbon at 700 m depth (i.e. a correction of 900 years, see text for further information). All ages were then corrected from surface reservoir age of 600 years. Ages younger than 25 ka BP were calibrated using Calib 5.0 (Stuiver et al., 2005), using dataset of Hughen et al. (2004); older ages are calibrated using the equation of Bard et al. (2004). The ranges of calibrated ages for a 95.4% (2σ confidence level are indicated. For all ages, the probabilities (relative area under distribution) are 1. In same levels, or when the ages were overlapping within the 2σ errors, the calibrated ages have been averaged.

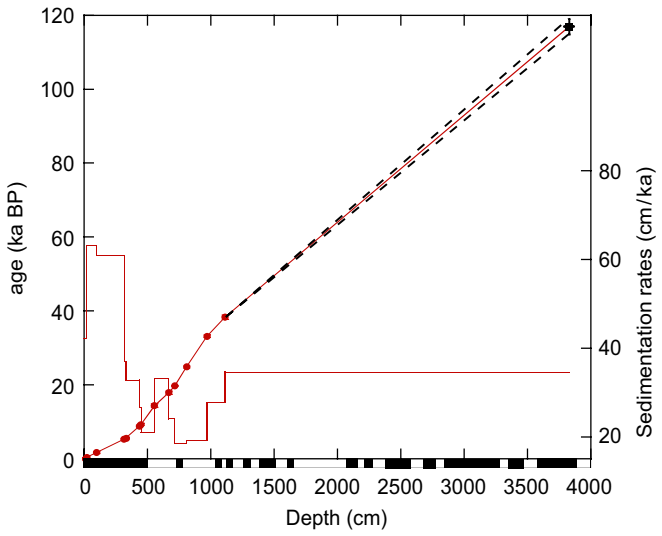

Fig. 7. Age/depth relationship along core MD0-2508: linear interpolation was used between the 16 ^{14}C calendar ages (dots include the 2σ error), and between the oldest ^{14}C calendar age and the age of the Blake excursion (115–122 ka BP) identified between 3800 and 3860 cm (black square). Inferred sedimentation rates are given in cm/ka (right axis) and the laminated intervals are indicated along depth (*X*-axis) by black rectangles.

by mineralisation of organic matter under dysoxic conditions) interacts with Fe^{2+} (released by iron bearing minerals) to form various iron sulphides: ferrimagnetic greigite (Fe_3S_4) and pyrrhotite (Fe_7S_8) constitute an intermediate stage of reduction (Fe III still present); paramagnetic pyrite (FeS_2) is the ultimate degree of reduction (Fe II only) (Berner, 1970).

In the laminated intervals of core MD02-2508, such reductive conditions are evidenced by laminae preservation (lack of bioturbation) which suggests low O_2 concentrations (van Geen et al., 2003) and high TOC and S contents (Fig. 6). Local enrichments of ferrimagnetic sulphides (Fig. 2) and presence of pyrite—indicated by weak values of the magnetic parameters and high S contents—indeed suggest that in these intervals, primary (magnetic) minerals have been partly dissolved.

In addition, overprints of the primary magnetic signal appear in three localised intervals (at 250–330 cm, 1200–1220 cm and 1280–1300 cm), where Fe and Ti enrichments are related to low magnetic concentrations. In these intervals, magnetic minerals dissolution can result in both (i) *in situ* authigenesis of pyrite (implying higher primary magnetic concentrations) and/or (ii) solubilisation, migration and accumulation of all elements (including Ti, despite its low sensitivity to redox conditions) at the depth of palaeoredox fronts.

8.1.3. *Varying terrigenous input*

Despite the evidence of diagenetic imprint on the magnetic signal, several arguments support the hypothesis that variations in magnetic concentration may reflect primarily the terrigenous input variations. At first, the fact that Fe, Ti, K and Si contents as well as the magnetic concentrations are enhanced at the transition I/II and in part II indicates the affinity of the Fe and Ti oxi-hydroxides with the lithogenic elements (Fig. 6). The preserved correlation of the potassium content with magnetic parameters in the interval 1200–1300 cm, despite a suspected diagenetic overprinting, reinforces this argument. Secondly,

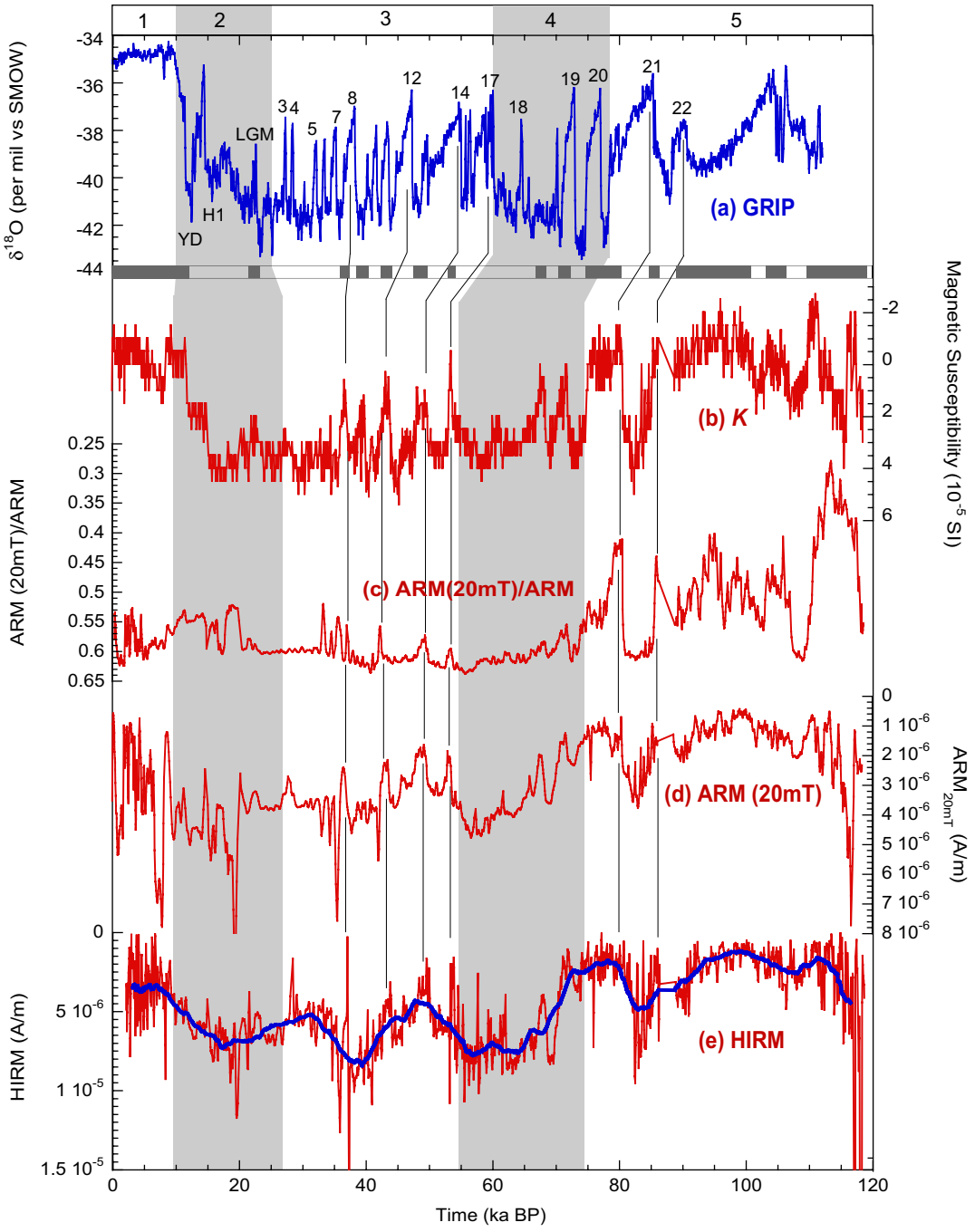

Fig. 8. Time variations of the magnetic parameters, compared to GRIP $\delta^{18}O$ record (a) (Grootes et al., 1993; Johnsen et al., 2001) over the last 120 ka. (b) *K*, (c) $ARM_{20\,mT}/ARM$, (d) $ARM_{20\,mT}$ and (e) HIRM are presented on inverse scales. Laminated intervals are represented as black rectangles along the *K* record. Concentration and grain size variations are placed in a global climate context by refeering the Marine Isotope Stages (MIS) (top panel; glacial MIS = grey). The correlation discussed in the text is shown as thin lines and the main climatic events are labelled: Younger Dryas (YD), Heinrich event 1 (H1, cited in the text as Oldest Dryas), Last Glacial Maximum (LGM) and the interstadials of the MIS3. The HIRM curve (thin red curve) was smoothed using a moving average on 70 points (thick blue curve).

the changes from high to low magnetic concentrations (and conversely) are gradual (i.e. transition I/II, Fig. 6) and do not correspond with boundaries of the laminated intervals, which would not be the case if the dissolution of iron oxides was the main modulating factor. Thirdly, the HIRM signal carried by haematite and goethite, minerals less sensitive to dissolution (Funk et al., 2004) shows oscillations of medium wavelength that are unrelated to both the biogenic content and the presence of laminations. Thus, we consider that it mainly reflects a terrigenous input signal. Finally, the similarity of the short and medium term variation of the $ARM_{20\,mT}$ (sensitive to fine-grained Ti-magnetite) and the HIRM suggests a common modulation, and demonstrates that variations of fine-grained

Ti-magnetite concentration depends on terrigenous input variations, despite their presumed higher sensitivity to reductive dissolution (Vigliotti et al., 1999; Larrasoaña et al., 2003) (Fig. 8d,e).

To conclude, we favour the hypothesis that both long-term behaviour (transitions between parts I, II and III) and rapid variations (in part II) of the magnetic mineral concentration reflect the first-order fluctuations of the terrigenous input. However, variation in diagenesis intensity between laminated and non-laminated facies may have amplified their initial contrasts. The medium wavelength variability, mainly visible in the HIRM signal is not related to TOC, nor to laminations, and therefore reflects the terrigenous signal.

8.2. Palaeoclimatic implications

The magnetic record of core MD02-2508 covers the last 120 ka with a temporal resolution of ~65 years, authorising the comparison with the highest resolution record of palaeoclimatic variations of the last glacial cycle, i.e. the Greenland Ice Core Project (GRIP) $\delta^{18}O$ record of atmospheric temperature variations (Grootes et al., 1993; Johnsen et al., 2001) (Fig. 8a). The largest amplitude variation of the magnetic concentration indices [magnetic susceptibility, $ARM_{20\,mT}$ and HIRM (Fig. 8b,d,e)] and grain size index $ARM_{20\,mT}/ARM$ (Fig. 8c) show a clear relationship with the major palaeoclimatic transitions of the upper Pleistocene: part I corresponds to the MIS I (Holocene), part II corresponds to MIS 2, 3 and 4 and part III corresponds to MIS 5. Therefore, weak terrigenous input characterised the interglacials MIS 1 and 5, while strong terrigenous input characterised glacials MIS 2, 3 and 4.

Superimposed on the glacial/interglacial variability, a short-term variability (10^3–10^4 years) is evidenced in transitions MIS 1–MIS 2 (transition I/II), MIS 4–MIS 5 (transition II/III) and MIS 3 and MIS 4. By analogy with the long-term variability, the magnetic mineral concentration documents a shorter term alternation between glacial-like and interglacial-like sedimentation styles. These magnetic signals (K, $ARM_{20\,mT}$ and HIRM) visually correlate with well-defined stadial/interstadial alternations of MIS 3, 4 and 5 in the GRIP $\delta^{18}O$ record. Despite obvious similarities, some discrepancies must be acknowledged. First, the time lags increase from 2 to 5 ka between 40 and 80 ka BP, i.e. in the part of our record dated by interpolation; the lags may thus be assigned to dating uncertainties (Fig. 8). During Termination I (10–20 ka BP), terrigenous input variations do not mirror the isotopic composition changes in GRIP: (i) the Younger Dryas and Bölling-Ällerod periods are weakly expressed and (ii) the Oldest Dryas and the LGM are grouped in a single strong magnetic susceptibility feature. This gradual profile of deglaciation has already been reported in Mo and Cd concentration records from a nearby location (Dean et al., 2006).

A common mechanism can be invoked to explain the short- and long-term changes in terrigenous input at core location. During glacial and stadial times the extension of the ice sheet over North America imposed an arid and cold climate (Heusser, 1998; Zic et al., 2002), precluding vegetation development and soil formation, and favouring the erosion of continental surfaces. An increase of the transport efficiency, related to river competence may have also enhanced the fluvial input to the margin. Between glacial and interglacial as well as between stadial and interstadial states, the emersion (and submersion) of coastal surfaces by sea level variations might have also modulated the terrigenous sedimentation. Indeed, noticeable sea level variations during MIS 3 and 4 have been evidenced (Chappell, 2002; Siddall et al., 2003; Arz et al., 2007).

The time variations of terrigenous input in core MD02-2508 can then be compared with changes in organic carbon content, showing the same pattern as the TOC record from a nearby core which Ortiz et al. (2004) interpreted as a proxy for primary productivity in surface waters. This suggests higher primary productivity during periods of

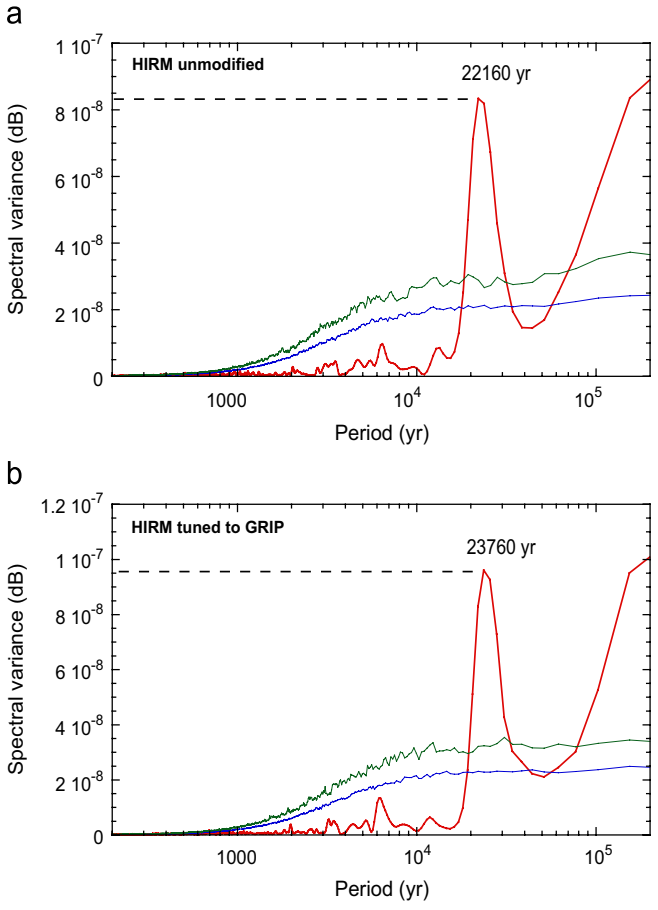

Fig. 9. Results of the spectral analysis of the raw HIRM record using the hardware Redfit (Lomb-Scargle Fourier transform). (a) HIRM record on the initial age model (see text and Fig. 7), (b) HIRM record tuned to GRIP chronology. In both cases, spectral variance is higher than the 95% (lowest blue line) and the 99% (upper green line) confidence levels.

reduced magnetic mineral input (Fig. 6). However, calculations of mass accumulation rate in the same core showed that variations of TOC, Mo and Cd concentration were actually driven by dilution with nonbiogenic matter (Dean et al., 2006). Our results support this conclusion since the terrigenous input was stronger at times of low concentration of TOC, Mo and Cd.

A medium term variability clearly appears in the HIRM record (Fig. 8e), reflecting the modulation of the haematite and/or goethite input. The arid conditions currently prevailing on the neighbouring land (particularly in northern Mexico and the Baja California peninsula) may favour the alteration of Ti-magnetite (contained in the andesitic and granitic cover) into haematite and/or goethite. In sediment cores located off the African and Asian deserts, these minerals were used to trace the aeolian input [e.g. from Africa to the Eastern Equatorial Atlantic (Bloemendal et al., 1988); from India to the Indian ocean (Bloemendal et al., 1993; Maher and Hounslow, 1999) and from Asia to the North Central Pacific (Yamazaki and Ioka, 1997)]. In core MD02-2508, the medium-term variability is only observed in the HIRM and is absent from the magnetic susceptibility (related to fluvial input). This further suggests that the winds might have been the main providers of haematite and/or goethite to the coring site. A spectral analysis of the HIRM record reveals that it is paced by a significant 22 ka period (Fig. 9a). The periodicity in the HIRM record is found to be more closely related to the equinoxial precession period (23.8 ka) after tuning the magnetic susceptibility record to the GRIP record for the time interval 40–80 ka BP (Figs. 9b and 10a,b). The tight correlation between the tuned HIRM record and the 23°N summer insolation variations (Laskar, 1990) suggests that the wind blown haematite/goethite input was strengthened (resp. weakened) during insolation minima (resp. maxima) (Fig. 10c,d). This indicates that

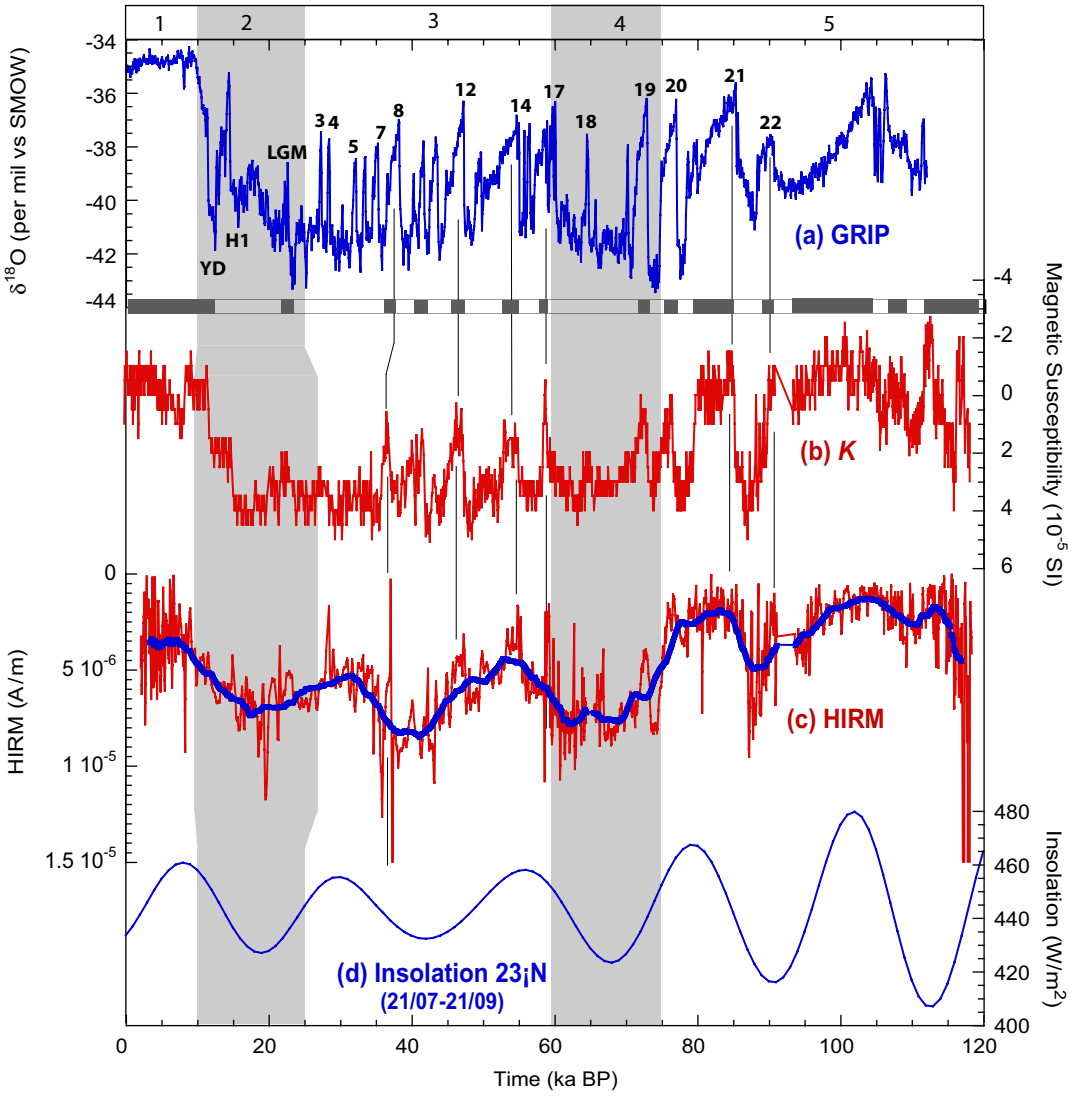

Fig. 10. Comparison of the GRIP $\delta^{18}O$ record (a) (Grootes et al., 1993; Johnsen et al., 2001) with time variation of *K* (b) and HIRM (c) tuned to GRIP chronology. Summer insolation at 23°N (Laskar, 1990) is also shown (d). Principal climatic features are indicated: MIS 1–5 on the top panel, interstadials of MIS 3, Younger Dryas (YD), Heinrich Event 1 (H1) and Last Glacial Maximum (LGM) along GRIP profile.

aridity over the nearby continental surfaces and/or wind strength followed the rhythm of the tropical insolation (driven by equinoxial precession), similar to the present climatic contrast between winter (arid, strong winds) and summer conditions (limited precipitation, weaker winds).

9. Conclusions

The analysis of the lithologic, magnetic and chemical properties of the sediment core MD02-2508 and the evidence of their narrow relationship with rapid palaeoenvironmental and palaeoclimatic changes on the continent suggest that the short, medium and long-term variations primarily reveal rhythms of the terrigenous minerals input. The contribution of diagenetic dissolution of the iron oxides, active in the laminated intervals, is however acknowledged as an amplifier of the primary magnetic signal.

The magnetic concentration and grain size vary following the glacial (stadials) and interglacial (interstadials) alternation over the last 120 ka, under direct control of: (i) extension of vegetation and soils (limiting erosion), (ii) efficiency of particle transport by rivers and winds and (iii) variations in emerged surfaces driven by sea level variations.

Two terrigenous mineral paths are hypothesised, relating Ti-magnetite to fluvial input and haematite and goethite to aeolian input. They followed two complementary regimes: (i) millennial-scale fluctuations of the fluvial transport are related to temperature variations at high latitudes, probably through the influence of the North American ice cap; (ii) periodical changes in the aeolian transport were slowly paced by tropical insolation, with maximum aridity and strong aeolian deflation during weak insolation periods, and monsoon-like warmer and wetter conditions during high insolation periods. Finally, this study reveals the influence of the low latitude insolation on the palaeoclimatological regimes in this region.

Acknowledgements

We wish to thank Yvon Balut (IPEV) and the team of the IMAGESVIII-MONA cruise (MD126 North American Margin) on board of the Marion Dufresne. The authors are also grateful to Michael Grelaud (CEREGE) for providing the spectral analysis and to Claude Degiovanni for the help on laser granulometer (Centre d'Océanologie de Marseille). Two anonymous reviewers are also acknowledged for their constructive comments, which helped to improve the manuscript. This work was performed in the frame of the Ph.D. Thesis of C.L.B. under the supervision of N.T. and L.V. Organic carbon and carbonate measurements were done by G.L. in the frame of a Ph.D. Thesis directed by L.V., K.T. and E.B.; K.T. performed the ICP measurements; L.B. was the organiser and chief scientist of the Images Cruise MD-126 MONA and was the principal investigator of the MD02-2508 coring site.

References

Arz, H.W., Lamy, F., Ganopolski, A., Nowaczyk, N., Pätzold, J., 2007. Dominant northern hemisphere climate control over millenial-scale glacial sea-level variability. Quaternary Science Reviews 26, 312–321.

Bard, E., Rosteck, F., Ménot-Combes, G., 2004. Radiocarbon calibration beyond 20,000 ^{14}C yr B.P. by means of planktonic foraminifera of the Iberian Margin. Quaternary Research 61, 204–214.

Beaufort, L., members of the scientific party, 2002. MD126-IMAGES VIII Marges Ouest Nord Américaines MONA Cruise Report. Institut Paul Emile Victor, Plouzané, France.

Berger, R., Taylor, R.E., Libby, W.F., 1966. Radiocarbon content of marine shells from the California and Mexican West coast. Science 153, 864–866.

Berner, R.A., 1970. Sedimentary pyrite formation. American Journal of Science 286, 1–23.

Bloemendal, B., Lamb, B., King, J.W., 1988. Paleoenvironment implications of rock-magnetic properties of late Quaternary sediment cores from the Eastern Equatorial Atlantic. Paleoceanography 3, 61–87.

Bloemendal, J., King, J., Hunt, A., de Menocal, P., Hayashida, A., 1993. Origin of the sedimentary magnetic record at Ocean Drilling Program sites on the Owen ridge, Western Arabian Sea. Journal of Geophysical Research 98 (B3), 4199–4219.

Chappell, J., 2002. Sea level changes forced ice breackouts in the last Glacial cycle: new results from coral terraces. Quaternary Science Review 21, 1229–1240.

Dean, W.E., Zheng, Y., Ortiz, J.D., van Geen, A., 2006. Sediment Cd and Mo accumulation in the oxygen-minimum zone off western Baja California linked to global climate over the past 52 kyr. Paleoceanography 21, PA4209.

Fang, X.-M., Li, J.-L., Van der Voo, R., Mac Niocaill, C., Dai, X.-R., Kemp, R.A., Derbyshire, E., Cao, J.-X., Wang, J.-M., Wang, G., 1997. A record of the blake event during the Last Interglacial paleosol in the western loess plateau of China. Earth and Planetary Science Letters 146, 73–82.

Funk, J.A., von Dobeneck, T., Reitz, A., 2004. Integrated rock magnetic and geochemical quantification of redoxomorphic iron mineral diagenesis in Late Quaternary sediments from the Equatorial Atlantic. In: Wefer, G., Mulitza, S., Ratmeyer, V. (Eds.), The South Atlantic in the Late Quaternary: reconstruction of material budget and current systems. Springer-Verlag, Berlin-Heidelberg.

Grootes, P.M., Stuiver, M., White, J.W.C., Johnsen, S., Jouzel, J., 1993. Comparison of oxygen isotope records from the GISP2 and GRIP Greenland ice cores. Nature 366, 552–554.

Herbert, T.D., Shuffert, J.D., Andreasen, D., Heusser, L., Lyle, M., Mix, A., Ravelo, A.C., Stott, L.D., Herguera, J.C., 2001. Collapse of the california current during the glacial maxima linked to climate change on land. Science 293, 71–76.

Heusser, L.E., 1995. Pollen stratigraphy and paleoecologic interpretation of the 160-k.y. record from Santa Barbara Basin, California. In: Kennett, J. P., Baldauf, J. G., Lyle, M. (Eds.), Proceeding of the Ocean Drilling Program, Scientific Results. Ocean Drilling Program, College Station, TX, pp. 265–279.

Heusser, L., 1998. Direct correlation of millenial-scale changes in western North American vegetation and climate with changes in the California Current system over the past ~60 kyr. Paleoceanography 13, 252–262.

Hughen, C.A., Lehman, S., Southon, J., Overpeck, J., Marchal, O., Herring, C., Turnbull, J., 2004. ^{14}C activity and global carbon cycle changes over the past 50,000 years. Science 303, 202–207.

Jansen, J.H.F., Van der Gaast, S.J., Koster, B., Vaars, A.J., 1998. CORTEX, a shipboard XRF-scanner for element analyses in split sediment cores. Marine Geology 151, 143–153.

Jennerjahn, T.C., Ittekkot, V., Arz, H.W., Behling, H., Pätzold, J., Wefer, G., 2004. Asynchronous terrestrial and marine signals of climate change during Heinrich Events. Science 306, 2236–2239.

Johnsen, S.J., Dahl-Jensen, D., Gundestrup, N.S., Steffensen, J.P., Clausen, H.B., Miller, H., Masson-Delmotte, V., Sveinbjörnsdottir, A.E., White, J., 2001. Oxygen isotope and paleotemperature records from six Greenland ice-core stations: Camp century, Dye-3, GRIP, GISP2, Renland and NorthGRIP. Journal of Quaternary Science 16 (4), 299–307.

King, J.W., Banerjee, S.K., Marvin, J., 1983. A new rock magnetic approach to selecting sediments for geomagnetic paleointensity studies: application to paleointensity for the last 4000 years. Journal of Geophysical Research 88 (B7), 5911–5921.

Larrasoaña, J.C., Roberts, A.P., Stoner, J.S., Richter, C., Wehausen, R., 2003. A new proxy for bottom-water ventilation in the Eastern Mediterranean based on diagenetically controlled magnetic properties of sapropel-bearing sediments. Palaeogeography, Palaeoclimatology, Palaeoecology 190, 221–242.

Laskar, J., 1990. The chaotic motion of the solar system: a numerical estimate of the chaotic zones. Icarius 88, 266–291.

Lynn, R.J., Simpson, J.J., 1987. The California Current System: the seasonal variability of its physical properties. Journal of Geophysical Research 92 (C12), 12,947–12,966.

Maher, B.A., Hounslow, M.W., 1999. Paleomonsoon II: magnetic records of aeolian dust in Quaternary sediments of the Indian Ocean. In: Maher, B.A., Thompson, R. (Eds.), Quaternary Climates, Environments and Magnetism. Cambridge University Press, Cambridge, pp. 126–162.

Maher, B.A., Thompson, R., 1999. Quaternary climates, environments and magnetism. Press Syndicate of the University of Cambridge, Cambridge.

Marchitto, T.M., Lehman, S.J., Ortiz, J.D., Flückiger, J., van Geen, A., 2007. Marine radiocarbon evidence for the mechanism of deglacial atmospheric CO_2 rise. Science 316, 1456–1459.

Ortiz, J.D., O'Connell, S.B., DelViscio, J., Dean, W.E., Carriquiry, J.D., Marchitto, T., Zheng, Y., van Geen, A., 2004. Enhanced marine productivity off western North America during warm climate intervals of the past 52 ky. Geology 32, 521–524.

Ostlund, H.G., Craid, H., Broecker, W.S., and Spencer, D., 1987. GEOSECS Atlantic, Pacific, and Indian ocean expeditions 7. National Scientific Foundation, Washington, D.C.

Peters, C., Thompson, R., 1998. Magnetic identification of selected natural iron oxides and sulphides. Journal of Magnetism and Magnetic Material 183, 365–374.

Peterson, L.C., Haug, G.H., Huguen, K.A., Röhl, U., 2000. Rapid changes in the hydrological cycle in the tropical Atlantic during the last glacial. Science 290, 1947–1951.

Roberts, A.P., 1995. Magnetic properties of sedimentary greigite (Fe_3S_4). Earth and Planetary Science Letters 134, 227–236.

Rochette, P., Vadeboin, F., Clochard, L., 2001. Rock magnetic applications of Halbach cylinders. Physics of the Earth and Planetary interiors 126, 109–117.

Siddall, M., Rohling, E.J., Almogi-Labin, A., Hemleben, C., Meischner, D., Schmelzer, I., Smeed, D.A., 2003. Sea-level fluctuations during the last glacial cycle. Nature 423, 853–858.

Stuiver, M., Reimer, P.J. and Reimer, R., 2005. Calib 5.0, 〈http://calib.qub.ac.uk/calib/manual/〉.

Suits, N.S., Arthur, M.A., 2000. Sulfur diagenesis and partitioning in Holocene Peru shelf and upper slope sediments. Chemical Geology 163, 219–234.

Talley, L.D., 1993. Distribution and formation of North Pacific Intermediate Water. Journal of Physical Oceanography 23, 517–537.

Thomas, A.C., Carr, M.-E., Strub, P.T., 2001. Chlorophyll variability in Eastern boundary currents. Geophysical Research Letters 28 (18), 3421–3424.

Thompson, R., Oldfield, F., 1986. Environmental Magnetism. Allen & Unwin, London.

Thouveny, N., Moreno, E., Delanghe, D., Candon, L., Lancelot, Y., Shackleton, N.J., 2000. Rock magnetic detection of distal ice-rafted debries: clue for the identification of Heinrich layers on the Portuguese margin. Earth and Planetary Science Letters 180, 61–75.

Thouveny, N., Carcaillet, J., Moreno, E., Leduc, G., Nerini, D., 2004. Geomagnetic moment variations and paleomagnetic excursions since 400 kyr BP: a stacked record from sedimentary sequences of the Portuguese Margin. Earth and Planetary Science Letters 219, 377–396.

Tric, E., Laj, C., Valet, P.-P., Tucholka, P., Paterne, M., Guichard, F., 1991. The Blake geomagnetic event: transitional geometry dynamical characteristics and geomagnetic significance. Earth and Planetary Science Letters 102, 1–13.

van Geen, A., Fairbanks, R.G., Dartnell, P., McGann, M., Gardner, J.V., Kashgarian, M., 1996. Ventilation changes in the Northeast Pacific during the last deglaciation. Paleoceanography 11 (5), 519–528.

van Geen, A., Zheng, Y., Bernhard, J.M., Cannariato, K.G., Carriquiry, J.D., Dean, W.E., Eakins, B.W., Ortiz, J.D., Pike, J., 2003. On the preservation of laminated sediments along the Western margin of North America. Paleoceanography 18 (4), 1098.

Verardo, D.J., Froelich, P.N., McIntyre, A., 1990. Determination of organic carbon and nitrogen in sediments using the Carlo Erba N-1500 analyser. Deep Sea Research 37 (1), 157–165.

Vigliotti, L., Capotondi, L., Torii, M., 1999. Magnetic properties of sediments deposited in suboxic-anoxic environments: relationship with biological and geochemical proxies. In: Tarling, D.H., Turner, P. (Eds.), Paleomagnetism and Diagenesis in Sediments, Geological Society, London, Special publications, No. 151, pp. 71–83.

Yamazaki, T., Ioka, N., 1997. Environmental rock-magnetism of pelagic clays: Implication for Asian eolian input to the North Pacific since the Pliocene. Paleoceanography 12 (1), 111–124.

Zaitsev, O., Cervantes-Duarte, R., Montante, O., Gallegos-Garcia, A., 2003. Coastal upwelling activity on the Pacific shelf of the Baja California peninsula. Journal of Oceanography 59 (3), 489–502.

Zic, M., Negrini, R., Wigand, P.E., 2002. Evidence of synchronous climate change across the Northern Hemisphere between the North Atlantic and the northwestern Great Basin, United States. Geology 30, 635–638.